ANTARES-Site/1999-002

Simulation of ^{40}K signals

Jürgen Brunner

1 Introduction

Optical modules which are operated in sea water register a large amount of signals originating from bioluminescence and from radioactive decays. The understanding of these signals is of crucial importance in designing a large scale experience.
Biological activity is known to produce light in an incoherent way. This means photons are detected on a 1 photo-electron basis and they arrive uncorrelated on time scales of a few nanoseconds. However radioactive decays may produce many photons within 1 nsec giving raise to higher amplitudes on a single photomultiplier or tight coincidences on neighbouring photomultipliers. The aim of this note is to describe the simulation of signals from ^{40}K decays and to determine count rates of single 8" and 10" photomultipliers at different amplitude thresholds as well as coincidence rates for various geometries. The spatial as well as the time distributions of the signals are evaluated.

2 Decay generator

^{40}K has two major decay branches:

- β^- decay with 89.3% probability and a kinetic endpoint energy of $Q = 1.311$ MeV
- Electron capture, with 10.7% probability, followed by a γ emission of $E_\gamma = 1.46$ MeV

Both decay modes have been simulated. The standard β^- spectrum has a shape according to

$$\frac{dN}{dE} \approx p \cdot (E + m_e) \cdot (Q - E)^2 \tag{1}$$

with p, E the electron momentum and kinetic energy and m_e the electron mass. For the ^{40}K decay two corrections are necessary:

- The Coulomb correction factor which accounts for the distortion of the electron wave function due to the nuclear Coulomb field.
- The spin correction factor which applies to transitions with a high change in spin. For the decay ^{40}K$\rightarrow^{40}$Ca spin changes by 4 units which is the main reason for the long lifetime of this isotope.

Both corrections shift the spectrum towards higher electron energies as shown in figure 1 in comparison to the standard shape described by Eq. 1.
To obtain total event rates the decay rate of ^{40}K in sea water is needed. All necessary ingredients are summarised in the Appendix. A rate of 13,750 decays per m^3 per sec has been derived.

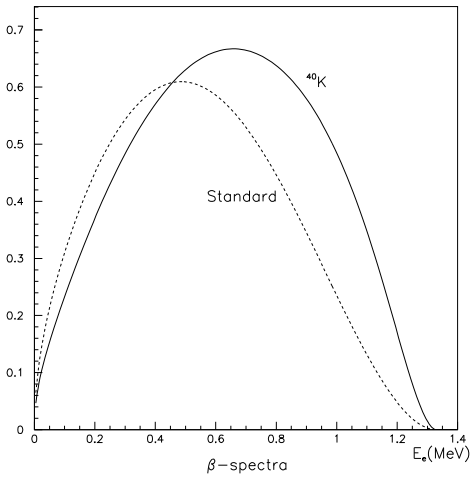

Figure 1: Deviation of ^{40}K β-spectrum compared to a standard β-spectrum without corrections

3 Cherenkov light generation

The produced particles (e^- or γ) are generated isotropically in a spherical shell around the photomultiplier arrangement. For tracking and secondary particle production the particles are passed to GEANT 3.21. To reach an acceptable resolution concerning the Cherenkov light production the maximal allowed fractional energy loss has been tuned to obtain an average step sizes of about 50-100 μm. The Cherenkov light cones per step are calculated by the corresponding GEASIM routine GUSTEP. Figure 2 shows the track length distributions separately for electrons and gammas. The electrons travel on average 2.3 mm. It does not produce secondary (shower) particles above Cherenkov threshold. The fine structure in the distribution is due to the finite step size, mentioned above. The gammas travel on average 68 cm and produce about two Compton electrons above the Cherenkov threshold.
Cherenkov light is generated in a wavelength region between 300 and 600 nm. Figure 3 illustrates the total number of photons produced over the whole active track length of the charged particles. The left plot shows the distribution for decays which produce at least one Cherenkov photon, 84% of all decays. On average 39 photons are produced. The fine structure at low photon numbers is again due to the GEANT step size. Taking into account the $1/\lambda^2$ dependence of Cherenkov light production one can easily find the following distribution of the produced photons in narrower wave length bins:

300-400 nm	50%
400-500 nm	30%
500-600 nm	20%

The right plot in figure 3 gives the photon number distribution for decays which produce a hit on an photomultiplier. The average number of produced photons for this sample is 70. At this

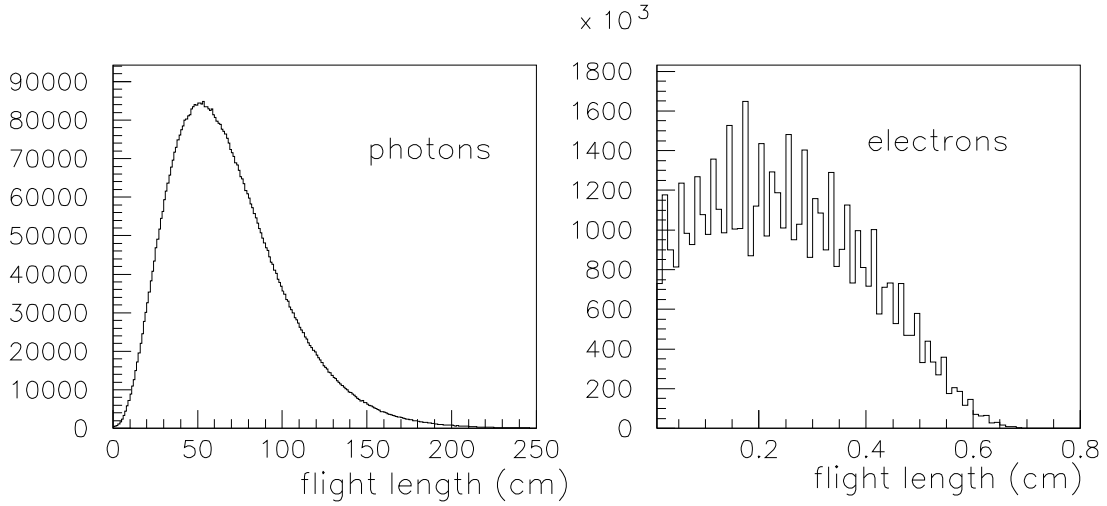

Figure 2: Flight length distribution of photons and electrons from ^{40}K decay

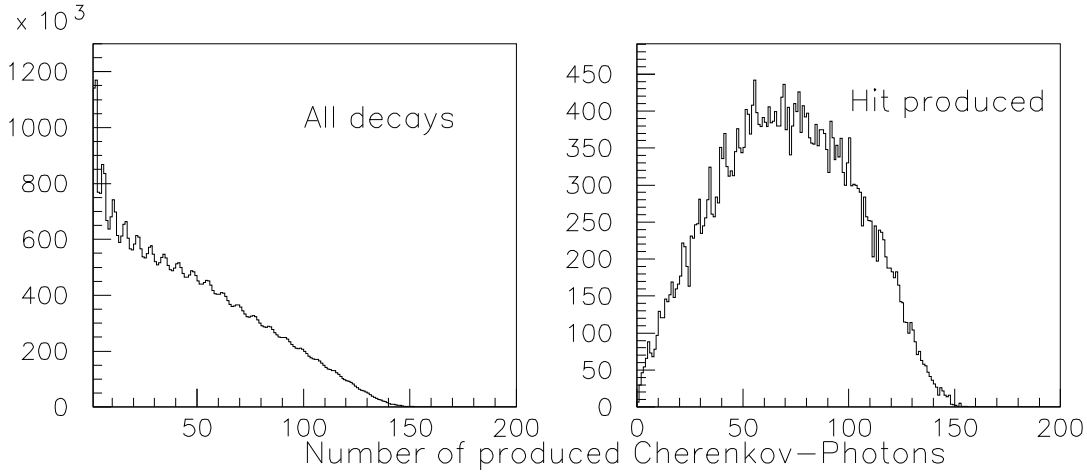

Figure 3: Number of produced Cherenkov photons between 300 and 600 nm: Left - For all decays; Right - For decays which produced a hit on a photomultiplier

moment water and photomultiplier parameters become important. The present simulation uses the wave length dependence of the

- attenuation length in sea water
- transmitivity of Benthos sphere and gel
- quantum efficiency of Hamamatsu phototubes

as illustrated on figure 5.4 of [1]. The maximal attenuation length is set to 55 m, scattering is neglected. An effective area of the photomultipliers of 280 cm^2 is used for the 8" tube. For the 10" photomultipliers two values are simulated: 440 cm^2 (10"A) which is just $(10/8)^2$ larger than the 8" value and 480 cm^2 (10"B) to match the result of Gamelle measurements where 55 photo-electrons have been observed from muons at 1 m distance [2]. These numbers include effects of collection efficiency and shadowing by the mu-metal shield.
The angular response has been parametrised according to figure 5.5 of [1]. All these parametrisations are also used in full scale physics simulations of ANTARES like GEASIM, DADA or KM3.
All distributions and values mentioned above have an uncertainty which is poorly known. They will contribute to an overall systematic error of the results presented in the following. The size of this error is estimated to be about 20% with main contributions from the effective area and the angular response of the photomultipliers.

4 Single rates

The simulation has been done in spherical shells of 0.2-5 m, 5-10 m, 10-20 m and 20-40 m around the photomultiplier and $6 \cdot 10^7$ decays have been simulated in each. This refers to 9 sec of real time for the inner shell and 20 msec for the outer shell. Figure 4(left) shows the radial distributions of the decays which produce at least one photo-electron. The low value of the first bin is due to the Benthos sphere of 21 cm radius where neither decays nor Cherenkov photon production has been allowed. The large error bars for bigger radius indicate the poor statistics for these bins. An extrapolation towards even larger radius is necessary to obtain precise results. It will be done analytically.
Apart from some global normalisation the radial dependence of the counting rate can be calculated on the basis of the wavelength dependence of the water attenuation length $L(\lambda)$ and the combined wavelength dependence of quantum efficiency, glass and gel transmitivity $f(\lambda)$ according to Eq. 2.

$$N(r) \sim \int \exp[-r/L(\lambda)] \cdot f(\lambda)/\lambda^2 d\lambda \tag{2}$$

Due to the necessary wavelength integration $N(r)$ will not be an exact exponential function. This can be illustrated by extracting the effective radius dependent attenuation length $L_0(r)$ according to Eq. 3.

$$L_o(r) = -N(r) \left[\frac{\partial N(r)}{\partial r}\right]^{-1} \tag{3}$$

Figure 4(right) shows that this effective attenuation length increases from 25 m for very short distances to 55 m at infinite distance from the photomultiplier. This can be understood in the

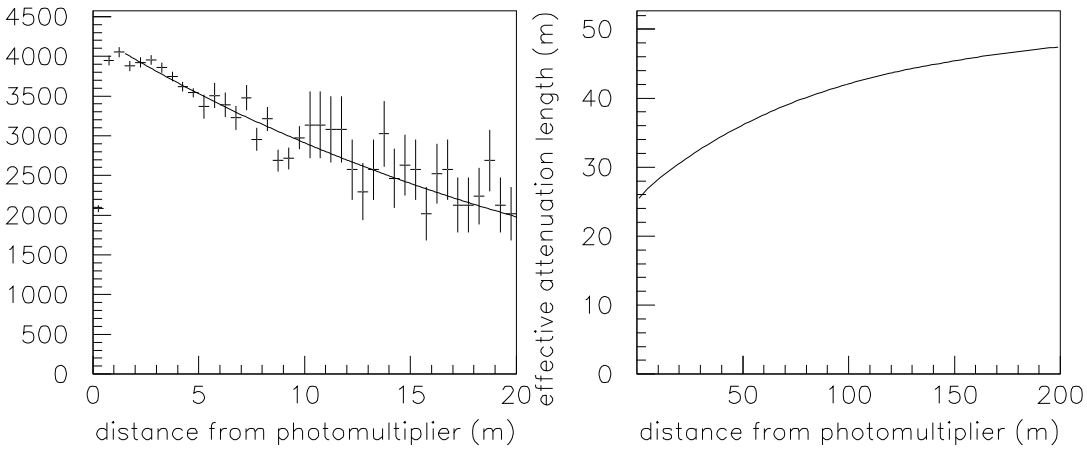

Figure 4: Left - Contribution of different radial distances to the count rate of a single photomultiplier. The fitted line follows Eq. 2; Right - Variation of the effective attenuation length with distance from the photomultiplier according to Eq. 3

following way: Very close to the photomultiplier a broader wavelength region with on average fast attenuation contributes to the signal. As the distance increases, only the region with highest attenuation length survives.

photo-electron threshold	rate 8"	rate 10"A	rate 10"B
npe ≥ 1	18 $\pm$ 2 kHz	27 $\pm$ 3 kHz	30 $\pm$ 3 kHz
npe ≥ 2	45 $\pm$ 2 Hz	94 $\pm$ 3 Hz	110 $\pm$ 4 Hz
npe ≥ 3	6.0 $\pm$ 0.8 Hz	12 $\pm$ 1.0 Hz	16 $\pm$ 1.3 Hz
npe ≥ 4	2.4 $\pm$ 0.5 Hz	3.8 $\pm$ 0.6 Hz	5.0 $\pm$ 0.8 Hz

Table 1: Counting rates of 8" and 10" photomultipliers for different photo-electron thresholds. The errors are statistical.

Applying the correction towards infinite distances following Eq. 2 the total counting rates are obtained. They are given in table 1. For 8" PMs one can compare these rates with results obtained at tests 1.6-1.8 [3]. Due to the additional contribution from bioluminescence only an upper limit for the ^{40}K decay rate could be derived from the minimal count rate. This minimal rate was found to be 17 kHz which agrees well with the 18 kHz found here. Furthermore count rates at a threshold of 2 pe have been measured. A value of about 300 Hz has been quoted. However it is dominated by the tail of the 1 pe distribution and random coincidences. From the present simulation one expects a contribution to this rate from the real 2 pe signal of 22 Hz,

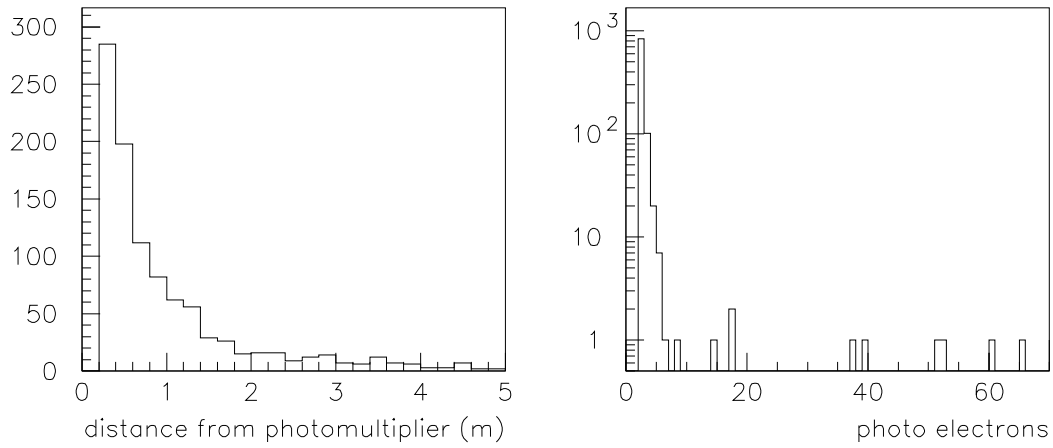

Figure 5: Multi-photo-electron hits: left - Distribution of radial distances of decays from the photomultiplier; right - Amplitude distribution

less than 10% of the measured rate.
The radial distribution of the rates are equal for the different photomultiplier types. The counting rates at the 1 pe level scale like the effective areas of the photomultipliers.
The contribution of the electron capture decay mode to the observed signal is 18%, whereas the branching ratio for this mode is only 10%. This means Cherenkov photons are more efficiently produced starting from the 1.46 MeV photon.
Increasing the photo-electron cut to 2 pe decreases the counting rate by more than factor 200 and changes dramatically the radial distribution of the hits shown in figure 5. It has been verified that the contribution from distances larger than 5 m is less than 1%. Therefore no correction for the extrapolation towards infinite distances has to be applied. The expected counting rates are again given in table 1 together with rates at even higher photo-electron levels. The ratios between different photomultiplier rates are roughly equivalent to the ratio of the squares of their effective areas. The amplitude distribution of all multi-pe hits is given in figure 5. Very rarely (about 0.1 Hz for 10"B) one will observe very high signals, up to 100 photo-electrons.

5 Coincidence rates

The geometry of tests 1.6/1.7 and 1.8 with 8" photomultipliers as described in [3] as well as test 1.10 with 10" photomultipliers has been simulated. Moreover a setup with 2 photomultipliers looking 45^o outwards as described in [1] has been simulated. The positions and directions of the photomultipliers for the different setups are summarised in table 2. For figure 7 and table 3 the coincidences between PM2 and PM3 of the "slanted" setup have been selected. The rate of triple coincidences is unmeasurably low.

setup		positions (x,y,z)			direction cosines		
1.6 / 1.7	PM1	0	0	0.3 m	1	0	0
	PM2	0.55 m	0	0	0	0	1
1.8 / 1.10	PM1	-0.7 m	0	0	0	0	1
	PM2	0.7 m	0	0	0	0	1
slanted	PM1	0	-a	0	0	$-\sqrt{(2)}/2$	$-\sqrt{(2)}/2$
	PM2	$\sqrt{(3)}/2\cdot$ a	a/2	0	$\sqrt{(6)}/4$	$\sqrt{(2)}/4$	$-\sqrt{(2)}/2$
	PM3	$-\sqrt{(3)}/2\cdot$ a	a/2	0	$-\sqrt{(6)}/4$	$\sqrt{(2)}/4$	$-\sqrt{(2)}/2$

Table 2: Geometries for the different PM setups (a=0.8m)

The simulation has been done in spherical shells of 0.2-2.5 m and 2.5-5 m around the photomultiplier setup and $6 \cdot 10^7$ decays have been simulated in each. This refers to 72 sec of real time for the inner shell and 10 sec for the outer shell producing sufficient statistics to detect data rates of a few Hz reliably. For tests 1.6/1.7 decays farther than 5 m from the photomultipliers do not contribute to the coincidence rates. This is not the case for tests 1.8/1.10 and the setup with slanted PMs. Figure 6 illustrates the decay distribution with respect to the centre of gravity between the two photomultiplier for test 1.10. An exponential function fits well the distribution beyond 1 m with an attenuation length of 1.8 m. This means the observed rates within 5 m have to be corrected by 10% to obtain the total rates. The same correction applies to test 1.8 whereas for the slanted-PM setup one has to add 30% from far decays. The corrected rates are

Geometry	rate npe ≥ 1	rate mixed	rate npe ≥ 2
1.6/1.7 (8")	28 $\pm$ 1 Hz	1.6 $\pm$ 0.2 Hz	0.16 $\pm$ 0.05 Hz
1.8 (8")	12 $\pm$ 2 Hz	0.3 $\pm$ 0.1 Hz	$<$ 0.02 Hz
1.10 (10"A)	29 $\pm$ 3 Hz	0.6 $\pm$ 0.1 Hz	$<$ 0.04 Hz
1.10 (10"B)	37 $\pm$ 3 Hz	1.0 $\pm$ 0.2 Hz	$<$ 0.04 Hz
slanted (10"A)	7 $\pm$ 2 Hz	$<$ 0.1 Hz	$<$ 0.04 Hz
slanted (10"B)	9 $\pm$ 3 Hz	$<$ 0.2 Hz	$<$ 0.04 Hz

Table 3: Coincidence rates for different setups and photo-electron thresholds. 'Mixed' means the first photomultiplier has a threshold at 1 pe and the second at 2 pe. The errors are statistical.

summarised in table 3. The rates at the 1 pe level can be easily compared to measurements [3] as coincidence rates are dominated by ^{40}K decays. For test 1.8 the simulation results agree well with the measured value of 11 Hz. There is a discrepancy for tests 1.6/1.7 where 19 Hz have been measured, however the measurements have a large error due to the presence of α-sources during the tests. At the 2 pe level the rates are too small to be derived within the present statistics for most of the setups, therefore only upper limits are derived. These limits are in agreement with the non-observation of coincidences at the 2 pe level at tests 1.6-1.8.
Comparison of results from setups with identical geometry but different photomultiplier characteristics allow to study the influence of the effective area on the coincidence rates. The ratios of their count rates vary as the ratio of the squares of their effective areas.

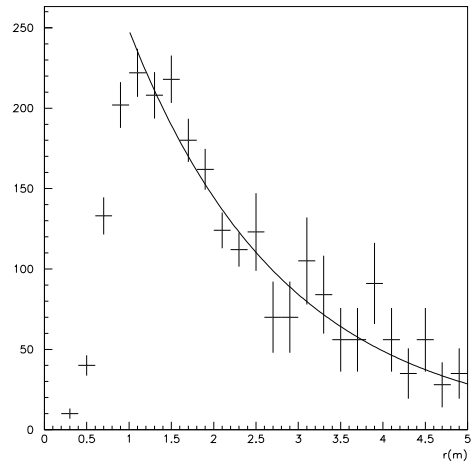

Figure 6: Distribution of radial distances of decays from the centre of gravity between the photomultipliers for test 1.10. The solid line represents an exponential fit with an "attenuation length" of 1.8 m

Figure 7 shows how the decays are arranged around the photomultipliers and how the arrival times of the two coincidence hits differ. These time distributions would be visible on top of the flat time difference distribution from random coincidences.

6 Conclusion

Results of single count rates and coincidence rates for different photomultipliers and different geometries have been derived. As far as experimental data are available the agreement is satisfying. On the basis of the present results one could decide whether a more sophisticated simulation of ^{40}K signals in the main Monte Carlo programs of ANTARES is necessary for a given geometry and photomultiplier choice.

References

[1] ANTARES proposal, June 1999.

[2] H.Lafoux, private communication.

[3] N.Palanque-Delabrouille, ANTARES-Site-1998-002.

[4] V.Bertin, private communication.

[5] A. Ivanoff, *Introduction a'l Oceanographie*, Paris (1972) p.18.

[6] http://www.shef.ac.uk/chemistry/web-elements/index.html

[7] http://hpngp01.kaeri.re.kr/CoN/index.html

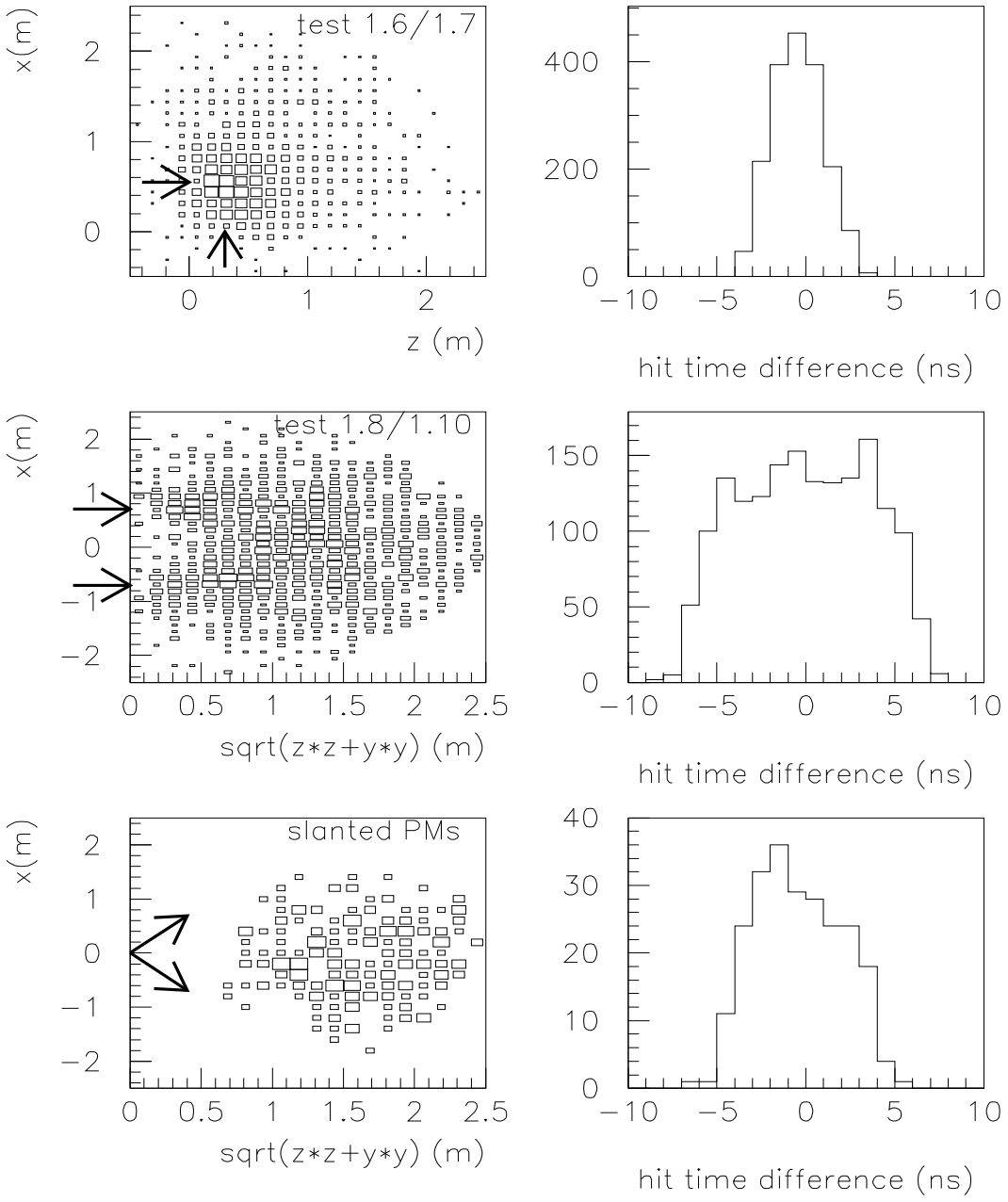

Figure 7: left - Distribution of decay points in the plane of the two photomultipliers, the arrow indicate their positions and orientations; right - Time differences between the two coincidence hits

Appendix - Radioactive decays in sea water

The salt content of the Mediterranean Sea at the ANTARES site has been measured to be 3.845% [4]. The Potassium contribution to the salinity is stable at 1.11% [5]. From these two values the mass fraction of Potassium in the sea water has been derived. The other elements have been taken from a database, which describes the chemical composition of average ocean water [6]. The lifetimes and isotope abundances are taken from an isotope table [7].
The decay rate per volume and time for a given isotope can be calculated in the following way:

$$N = r_m \cdot r_I \cdot \frac{ln2}{\tau} \cdot \frac{N_A}{A}\rho \tag{4}$$

where r_m denotes the mass fraction of the element in ocean water; r_I the isotope abundance of the radioactive isotope; τ the half-life of the isotope; **A** the atomic mass of the element; ρ the density of sea water at the ANTARES site (1.038 g/cm^3) and N_A is Avogadro's number. Table 4 summarises all relevant numbers from known natural radioactive decays in sea water. It

Isotope	A	r_m	r_I	τ (years)	Bq per m^3	Q (MeV)
^{40}K	39.1	$4.27 \cdot 10^{-4}$	$1.170 \cdot 10^{-4}$	$1.277 \cdot 10^{9}$	13,750	1.33
^{238}U	238.0	$3.30 \cdot 10^{-9}$	$0.993 \cdot 10^{0}$	$4.468 \cdot 10^{9}$	40 ($\times$6)	many $*$
^{87}Rb	85.5	$1.20 \cdot 10^{-7}$	$0.278 \cdot 10^{0}$	$4.750 \cdot 10^{10}$	110	0.28
^{235}U	238.0	$3.30 \cdot 10^{-9}$	$0.720 \cdot 10^{-2}$	$7.038 \cdot 10^{8}$	1.9 ($\times$4)	many $*$
^{187}Re	186.2	$1.00 \cdot 10^{-12}$	$0.626 \cdot 10^{0}$	$4.350 \cdot 10^{10}$	$1.0 \cdot 10^{-3}$	0.003
^{232}Th	232.0	$4.00 \cdot 10^{-14}$	$1.000 \cdot 10^{0}$	$1.405 \cdot 10^{10}$	$1.6 \cdot 10^{-4}$($\times$4)	many $*$
^{176}Lu	175.0	$1.50 \cdot 10^{-13}$	$2.590 \cdot 10^{-2}$	$4.000 \cdot 10^{10}$	$7.3 \cdot 10^{-6}$	1.19
^{138}La	138.9	$3.40 \cdot 10^{-12}$	$0.900 \cdot 10^{-3}$	$1.050 \cdot 10^{11}$	$2.8 \cdot 10^{-6}$	1.74
^{113}Cd	112.4	$5.00 \cdot 10^{-11}$	$0.122 \cdot 10^{0}$	$7.700 \cdot 10^{15}$	$9.3 \cdot 10^{-8}$	0.32
^{115}In	114.8	$1.00 \cdot 10^{-13}$	$0.957 \cdot 10^{0}$	$4.410 \cdot 10^{14}$	$2.5 \cdot 10^{-8}$	0.49
^{50}V	50.9	$1.50 \cdot 10^{-9}$	$2.500 \cdot 10^{-3}$	$1.400 \cdot 10^{17}$	$7.0 \cdot 10^{-9}$	2.21
^{180m}Ta	180.9	$2.00 \cdot 10^{-12}$	$1.200 \cdot 10^{-4}$	$1.200 \cdot 10^{15}$	$1.5 \cdot 10^{-11}$	0.85

Table 4: Natural radio isotopes in sea water, sorted according to their activity ($*$: For U and Th their whole decay chain contributes. Because production and decays along the chain are in equilibrium, the total decay rate is equivalent to the parent decay rate times the "chain length". For ^{238}U there are 6 β-decays in the chain, for ^{235}U and ^{232}Th there are 4).

is evident, that only few isotopes can produce significant signals for a water Cherenkov detector. Apart from ^{40}K, ^{238}U is worth noting. It has a long decay chain with many β-decays above the Cherenkov threshold. The combined rate of all β-decays in the ^{238}U chain is with 240 Bq/m^3 about a factor 50 lower than the ^{40}K rate but some of the decays produce much more Cherenkov photons than a ^{40}K decay. Therefore its contribution to higher order effects such as coincidence rates could be detectable.
Apart from radioactivity due to long lived isotopes there are some cosmogenic isotopes which are permanently reproduced by cosmic ray interactions. The most abundant one is ^{14}C. There are no data on its abundance in sea water available, but with an maximal β-decay energy of 0.156 MeV it is anyway below Cherenkov threshold and cannot contribute to a detectable signal. The same argument holds for ^{3}T with an endpoint energy as low as 18 keV.